Journal Name

ARTICLE

The structural landscape in 14-vertex clusters of silicon, M@Si_{14}: when two bonding paradigms collide.

Xiao Jin, Vaida Arcisauskaite and John E. McGrady*.

Received 00th January 20xx,
Accepted 00th January 20xx

DOI: 10.1039/x0xx00000x

www.rsc.org/

The structural chemistry of the title clusters has been the source of controversy in the computational literature because the identity of the most stable structure appears to be pathologically dependent on the chosen theoretical model. The candidate structures include a D_{3h}-symmetric 'fullerene-like' isomer with 3-connected vertices (A), an '*arachno*' architecture (B) and an octahedral isomer with high vertex connectivities typical of '*closo*' electron-deficient clusters (C). The key to understanding these apparently very different structures is the fact that they make use of the limited electron density available from the endohedral metal in very different ways. Early in the transition series the favoured structure is the one that maximises transfer of electron density from the electropositive metal to the cage whereas for later metals it is the one that minimises repulsions with the increasingly core-like d orbitals. The varying role of the d orbitals across the transition series leads directly to strong functional dependency, and hence to the controversy in the literature.

Introduction

The central position of silicon in contemporary electronic devices ensures that the chemistry and physics of silicon-based materials remains a very active field of research. The ultimate goal is to understand and improve the performance of solid-state devices, but a number of groups have begun to explore the properties of small gas-phase clusters which may provide an entry point for bottom-up growth of magnetic materials. The pioneering work in this area by Beck[1,2] described the formation of MSi_n clusters in a supersonic beam using group 6 metals (Cr, Mo and W) and a source of atomic silicon. Clusters with molecular formulae M@Si_{15} and M@Si_{16} proved to be particularly abundant, as they were in Ohara's[3] subsequent work using group 4 metals (Ti, Hf) and also in Neukermans and Lievens' wider study of the tetrels M@E_n, (M=Cr, Mn, Cu, Zn; E=Si, Ge, Sn, Pb).[4] When SiH_4 gas was used instead of elemental silicon, however, a series of partially hydrogenated clusters, M@$Si_nH_x^+$, was generated with maximum abundance at n = 14, 13 and 12 for Hf, Ta and W, respectively.[5] The highly reactive nature of these cluster species means that definitive structural information, in the form of diffraction data, is not available. Instead structural information can only be inferred from spectroscopic data, most notably the infra-red multiple photon dissociation experiments of Lievens and co-workers,[6,7] and from the large number of computational investigations that have been reported, principally using density functional theory. The most widely studied example from a computational perspective has been Cr@Si_{12},[8] primarily because it adopts a remarkable and unprecedented hexagonal prismatic geometry, the origins of which have been discussed by us[9-11] and by others.[12-17] Perhaps the most striking feature of the computational literature on these clusters is the extent to which the predicted equilibrium structures depend on the chosen methodology (functional, basis set *etc.*). A survey of the literature on the M@Si_{14} family, the subject of this paper, reveals that there is no clear consensus on the identity of the global minimum for many of the transition metals. For example, as far back as 2002 Hiura identified a 'fullerene-like' isomer (isomer A in Figure 1) as the global minimum of W@Si_{14} using the Perdew-Wang (PW91) functional with a Gaussian basis set.[18] In contrast, Kumar's group,[19] also using PW91 but with a plane-wave basis, concluded that a C_{2v}-symmetric structure (isomer B in Figure 1, labelled "arachno" for reasons that will be discussed later) was in fact the most stable. Lu and co-workers[20] argued for a third structure, a hexagonal prismatic structure with two Si atoms capping one hexagonal face (isomer D in Figure 1) based on the hybrid functional B3LYP. Similar ambiguities emerge for the lighter congener Cr@Si_{14}, where Khanna and co-workers argued for isomer B using the Perdew-Burke-Ernzerhof (PBE) functional,[17] while He's study[21] with B3LYP favoured the fullerene-like isomer A. Further to the right of the periodic table in group 8, we again find conflicting claims for the equilibrium structure: Khanna (PBE)[22] and Kumar (PW91)[23] have argued for the octahedral isomer C in Figure 1 for Fe@Si_{14}, while He (B3LYP)[21] has proposed the fullerene-like isomer, A. The only opportunity to tension these divergent predictions against experimental data comes from the infra-red multi-photon dissociation (IR-MPD)

Department of Chemistry, University of Oxford, South Parks Road, Oxford OX1 3QZ, UK

Electronic Supplementary Information (ESI) available: Full listing of Cartesian coordinates and total energies of the isomers described in Figure 2.

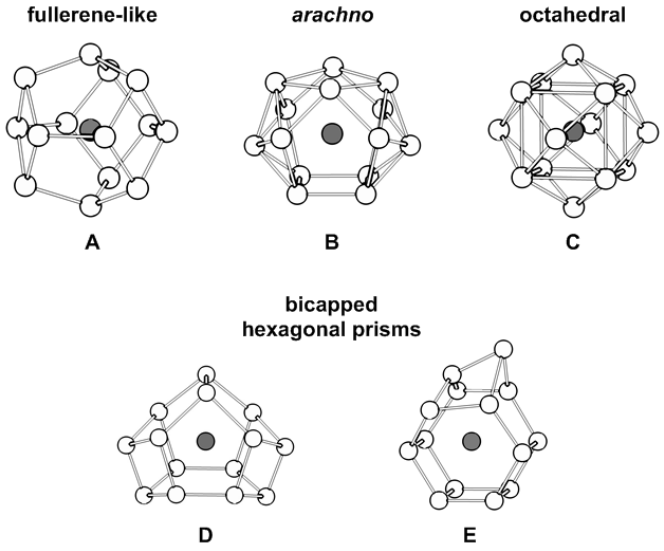

Figure 1. Structural types reported for the M@Si_{14} family.

experiments on the cationic clusters $[Mn@Si_{14}]^+$ and $[V@Si_{14}]^+$.[6,7] In both cases the vibrational spectrum is measured *via* the loss of a xenon tag, and structural evidence inferred by comparison with frequencies computed for different candidate structures. Three possibilities were identified for $[Mn@Si_{14}]^+$, the fullerene-like isomer A in both singlet and triplet states and a second distorted bicapped hexagonal prism, isomer E, this time with a dimer unit capping a square face. Calculations performed with the hybrid B3P86 functional indicate that these states all lie within 0.3 eV of each other, well below the threshold where a definitive conclusion about the equilibrium structure could reasonably be reached. Moreover, whilst the computed spectrum of each isomer showed some resemblance to the experiment, in no case was the match definitive. Nguyen and co-workers have also explored the relative stabilities of singlet and triplet states of $[Mn@Si_{14}]^+$ and isoelectronic $[Mn@B_3N_3Si_8]^+$ using both DFT and correlated *ab initio* approaches, concluding in both cases that a closed-shell singlet with the fullerene-like structure is the global minimum.[24,25] For the $[V@Si_{14}]^+$ analogue, with two fewer valence electrons, calculations with the BP86 functional identified isomer E as the global minimum, but with a triplet fullerene-like isomer (A) within 0.1 eV of the equilibrium structure. The authors again noted that whilst the vibrations of the lowest energy structure match some of the features of the measured spectrum, the agreement is not sufficiently strong to warrant a conclusive assignment.

It is abundantly clear from this brief survey that the choice of functional plays a defining role in the identity of the global minimum in these clusters, but there is precious little experimental evidence available to justify one choice over another. Indeed the search for new and improved functionals remains one of the most pressing issues in contemporary density functional theory.[26,27] Faced with this functional roulette, it becomes increasingly important to develop qualitative models of bonding that allow us at least to understand the factors that stabilise the different isomers. Armed with this information, we can then hope to understand why the choice of functional is so important in certain pathological cases, and to anticipate when similar problems might arise. Density functionals differ in their treatment of electron-electron repulsions (the exchange and correlation terms), and the choice is often particularly critical in first row transition metals, where the absence of a radial node in the 3d orbitals amplifies the electron-repulsions and, therefore, any inaccuracy in their treatment. If the bonding is qualitatively similar in the different isomers then we might anticipate that any errors should cancel, at least approximately, leaving the relative energies largely independent of the choice of functional. The fact that this is clearly not the case here suggests that the metal-based electrons play qualitatively different roles in the different isomers.

In recent papers we have attempted to establish the ground rules that determine structural preferences in the M@E_{10}[28] and M@E_{12}[9,10] families, where E is a tetrel element. For the early transition metals the preferred structures are prisms, either hexagonal (M@E_{12}) or pentagonal (M@E_{10}), both of which share features in common with the fullerene-like isomer, A (notably the 3-connected vertices). Later transition metals, in contrast, tend to adopt icosahedral (M@E_{12}) or bicapped square antiprismatic (M@E_{10}) structures whose high vertex connectivities are more reminiscent of isomers B and C. Thus despite the obvious differences in stoichiometry, the structural chemistry of the M@$Si_{10/12/14}$ families shows broad similarities that should be reconcilable within a common model of electronic structure.

Results and Discussion

Overview of the potential energy surface: To provide a framework for the discussion, we first show how the relative energies of the three different isomers (A, B, C in Figure 1) vary across the period for isovalent M@Si_{14} clusters, using three contrasting functionals that lie at the centre of the controversy in the literature: PBE, BLYP and B3LYP. Despite the arguments for isomers D and E in the literature, we have never found either of these to be the global minimum in any of the systems studied here, so they are not included in the plots. As a reference we have selected octahedral isomer C, the energy of which is set to zero in all four plots (green line). The source of the conflicting claims in the literature for the equilibrium structure of Cr@Si_{14} is immediately apparent from Figure 2: the B3LYP functional (plot c) places isomer A below B, as reported by Hiura[18] and He[21] while PBE (plot a) reverses the order, as reported by Kumar[19] and Khanna.[17] Equally, 64-electron Fe@Si_{14} lies close to the intersection of the curves for isomer A and C, and switching from PBE to B3LYP reverses the order. The plots also emphasise the important point, not immediately apparent from studies of individual molecules, that the relative stabilities of the various isomers vary smoothly as a function of electron count. Moreover the broad stability patterns are similar across all three plots, a-c, and should therefore be understandable in terms of fundamental

Journal Name

ARTICLE

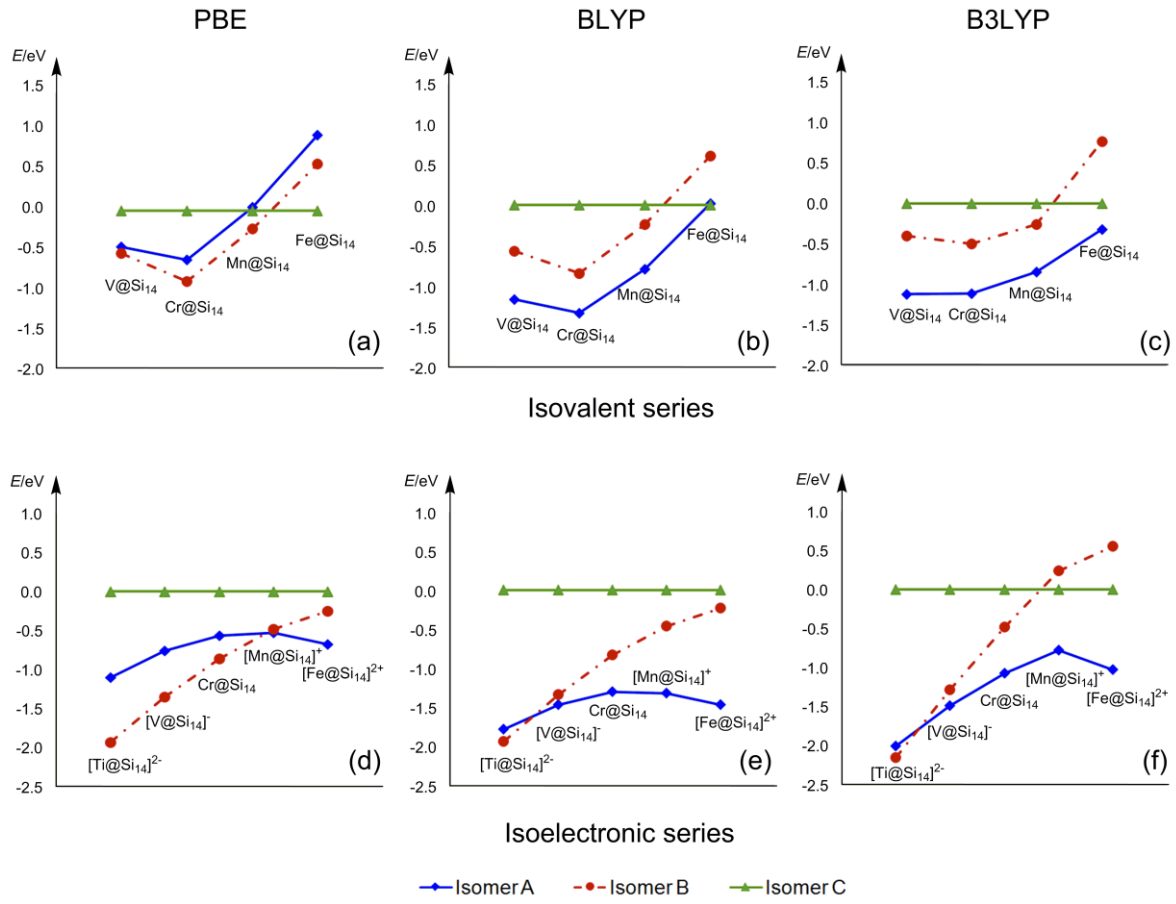

Figure 2. Relative energies of the three isomers, A, B and C shown in Figure 1 calculated using the PBE, BLYP and B3LYP functionals. The upper three plots show the relative energies for isovalent neutral species with varying d-electron counts (61-64 electrons) while the lower three plots correspond to a series of ions isoelectronic with $Cr@Si_{14}$ (62 valence electrons). Isomer C (green line) is taken as the energetic reference point in all cases.

principles of chemical bonding. A closer inspection of plots a-c reveals that the relative energies of isomers C (green) and B (red) are in fact relatively independent of functional, suggesting that these isomers share some common features, at least in terms of the electron-electron repulsions. The energy of isomer A (blue line), in contrast, floats up and down relative to B/C quite substantially, and this, ultimately, is the root cause of the different conclusions in the literature regarding the identity of the global minima. Furthermore, the energies of isomers A and B track each other closely across a wide range of electron counts, both reaching their maximum stability (relative to C) at 62-electron $Cr@Si_{14}$ in plots a-c. The 62-electron count is therefore somehow 'magic' for both isomer A and isomer B, although the strong functional dependence of their relative energies hints that the source of the magic may be different. We can obtain a different perspective on the balance between isomers A, B and C by considering the effect of changing the charge within an isoelectronic series with 62 valence electrons ($[Ti@Si_{14}]^{2-}$, $[V@Si_{14}]^{-}$, $Cr@Si_{14}$, $[Mn@Si_{14}]^{+}$, $[Fe@Si_{14}]^{2+}$), Figure 2 d-f. The most striking features of plots d-f is that isomer B (red line) is strongly destabilised relative to both A and C as the positive charge increases. The controversy over the global minimum of $Cr@Si_{14}$ does not, therefore, extend to isoelectronic $[Ti@Si_{14}]^{2-}$ or $[Fe@Si_{14}]^{2+}$, where isomers B and A, respectively, are the most stable for all functionals. The 3d orbitals on the metal become increasingly stabilised and radially contracted as the positive charge increases, from which we can conclude that the stability of isomer B is more heavily reliant on the availability of metal-based d-electron density than either isomer A or isomer C. Switching from the PBE functional to B3LYP replicates the effect of increasing positive charge, in so

much as the both changes destabilise isomer B relative to A, from which we can infer that the B3LYP functional also makes electron density on the metal less available to the Si_{14} cage. The CO stretching frequency of metal carbonyls is typically taken as measure of the availability of electron density from back-bonding, and it is striking that the computed frequency of the totally-symmetric CO stretch of $Cr(CO)_6$ is almost 100 cm^{-1} lower for the PBE functional (2081 cm^{-1}) than for B3LYP (2161 cm^{-1}).

The fact that the identity of the global minimum is so sensitive to the choice of computational method is perhaps unsurprising because in simple structural terms, isomers A, B and C are clearly very different: isomer A has 3-connected vertices and as a result is often referred to as 'fullerene-like' while isomers B and C appear more compact, their 4- and 5-connected vertices being reminiscent of the deltahedral electron-deficient boranes. Entirely different bonding paradigms have evolved in cluster chemistry to describe "fullerene-like" and "deltahedral" cases: the former is generally discussed in terms of aromaticity and the conjugated π system while the latter is very much the province of Wade's rules, and rarely do these two electronic structure models overlap. It appears that the particular case of these endohedral silicon clusters is an example where the two paradigms generate structures of comparable stabilities. In the next section, we examine the electronic structures of each of isomers A, B and C in isolation and show how they fit into the context of existing models of cluster electronic structure. We then attempt to bring the three together and understand why they are very similar, in energetic terms, in this class of compounds but not, apparently, in most other families of clusters.

"Fullerene-like" isomer A: Isomer A is often referred to as "fullerene-like" because of its resemblance to the archetypal fullerene, C_{60}, and indeed an isomer of 56-electron C_{14} has been identified with the same structure,[29] albeit 3 eV above the cyclic global minimum. 3-connected vertices are not, however, unique to fullerenes – they are also characteristic of electron-precise clusters, and isomer A has been identified as a stable minimum for the 70-electron phosphorus cluster, P_{14}.[30] Isomer A is therefore tolerant of a wide range of electron counts between 56 and 70, and so the adoption of a "fullerene-like" geometry is not *a priori* evidence of a "fullerene-like" electronic structure. The characteristic fullerene electron count of 4*n* (where *n* is the number of vertices) is made up of 3*n* electrons in a σ bonding framework and a further *n* electrons in a delocalised π system made up of linear combinations of radially oriented orbitals that lie perpendicular to the surface tangent. A truly "fullerene-like" Si_{14} cluster should therefore have a stable closed-shell electron count of 56, with seven filled Si-Si π orbitals and seven vacant π^* orbitals (4e″, 7e′, $6a_1'$, $4a_2''$ and $2a_2'$ on the right hand side of Figure 3, below). In electron-precise (70 electron) P_{14}, in contrast, these seven π^* orbitals are filled, and the fully occupied π/π^* manifold now constitutes the fourteen radially directed lone pairs of the electron-precise cluster. In $Cr@Si_{14}$, the six available d electrons on the metal participate strongly in back-bonding interactions, effectively populating three of the seven Si-Si π^* orbitals of fullerene-like Si_{14}, 4e″ and $6a_1'$, which are localised primarily in the polar regions of the cluster (centres I and II in the structure shown in Figure 3). The π^* orbitals of the Si_{14} fragment localised in the equatorial plane ($2a_2'$, 7e′), in contrast, remain vacant even in $Cr@Si_{14}$ (where they become $2a_2'$ and 8e′), and as a result the three equatorial Si-Si bond lengths are distinctly shorter than those in the polar region of the cluster (2.34 Å *vs* 2.43 Å). The phrase 'fullerene-like' is therefore somewhat misleading in $Cr@Si_{14}$, because despite the 3-connected nature of the vertices, meaningful Si-Si π bonding exists only in the equatorial plane. In summary, the interaction between the metal d electrons and the Si_{14} cage in isomer A can be understood in a classical synergic 'back-bonding' framework, where the Cr-Si bonding is enhanced at the expense of a weakening of the Si-Si π system. Critically, though, the encapsulated metal does not weaken the underlying Si-Si σ framework of 2-centre-2-electron bonds that drives the adoption of 3-connected isomer A. What, then, is 'magic' about the 62 electron count in $Cr@Si_{14}$: why can an endohedral $M@Si_{14}$ motif not accommodate up to 70 valence electrons as P_{14} does? Of the remaining four vacant Si-Si π^* orbitals that could act as potential acceptors, two simply lack the correct symmetry to match a metal d orbital ($2a_2'$ and $4a_2''$). The other two (7e′) could in principle accept electron density from occupied $d_{xy}/d_{x^2-y^2}$ orbitals, but would suffer from strong destabilising interactions with the occupied linear combination of Si-Si π orbitals, also with e′ symmetry (6e′ in Si_{14}, 7e′ in $Cr@Si_{14}$). The D_{3h}-symmetric architecture is therefore adapted to accommodate precisely 62 valence electrons of an endohedral cluster.

Journal Name

ARTICLE

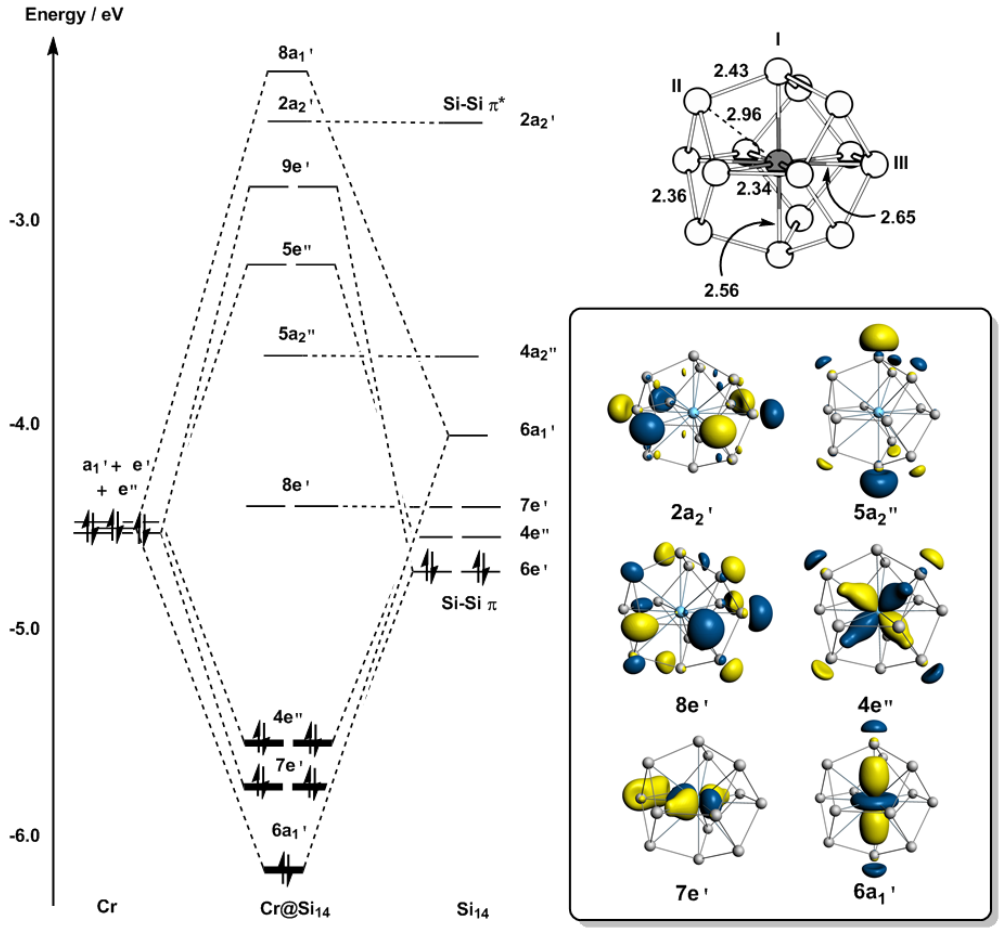

Figure 3 Kohn-Sham molecular orbitals for the "fullerene-like" isomer, A, of $Cr@Si_{14}$. The molecular orbital array is qualitatively very similar to that reported by Ngan *et. al.*[24]

"*arachno*" isomer B: We can now ask the same questions of the "arachno" isomer B for $Cr@Si_{14}$: can we understand its stability at a qualitative level in the context of existing bonding paradigms? We have already noted that the high connectivities of its vertices are characteristic of electron deficiency, and so it seems logical to look to Wade's rules, developed in the context of electron-deficient boranes, for inspiration. For a 14-vertex cluster, a 62-electron count corresponds to an *arachno*- architecture (62 = 4*n*+6), and so we should be able to post-rationalise isomer B as an *arachno*- cluster based on a 16- vertex parent polyhedron. Schleyer *et. al*[31] have predicted that the (unknown) *closo*- borane $[B_{16}H_{16}]^{2-}$ should adopt a D_{4d}-symmetric octa-capped square antiprismatic structure, and we find the isoelectronic $[Si_{16}]^{2-}$ cluster to have the same structure, irrespective of the chosen functional. The isolobal relationship between *closo*-$[Si_{16}]^{2-}$, *arachno*-$[Si_{14}]^{6-}$ and isomer B of $Cr@Si_{14}$ is summarised in the box in Figure 4. The neutral, empty Si_{14} cluster has a very narrow HOMO-LUMO gap and three closely-spaced vacant orbitals, $8b_1$, $7b_2$ and $5a_2$, immediately suggesting a first-order description of the cluster as $[Si_{14}]^{6-}$ and not a neutral cluster. In $Cr@Si_{14}$ these three low-lying vacant orbitals are stabilised by bonding interactions with the endohedral metal, generating the large HOMO-LUMO gap that is the signature of stable species. The $8b_1$, $8b_2$ and $4a_2$ orbitals in isomer B of $Cr@Si_{14}$ have *both* Cr-Si *and* Si-Si bonding character, a point best appreciated by considering the corresponding occupied orbitals in *arachno*-$[Si_{14}]^{6-}$ and *closo*-$[Si_{16}]^{2-}$, where the absence of a metal makes the in-phase relationship between nearest-neighbour Si centres easier to see. These electrons therefore have a dual role in electron counting terms, contributing to the 18-electron count of the metal *and* to the 4*n* + 6 count of the cluster: we have previously described this as a "jigsaw model" because the metal-based electron density locks the cluster together.[9,10] Isomer B is therefore uniquely tailored to

Journal Name

ARTICLE

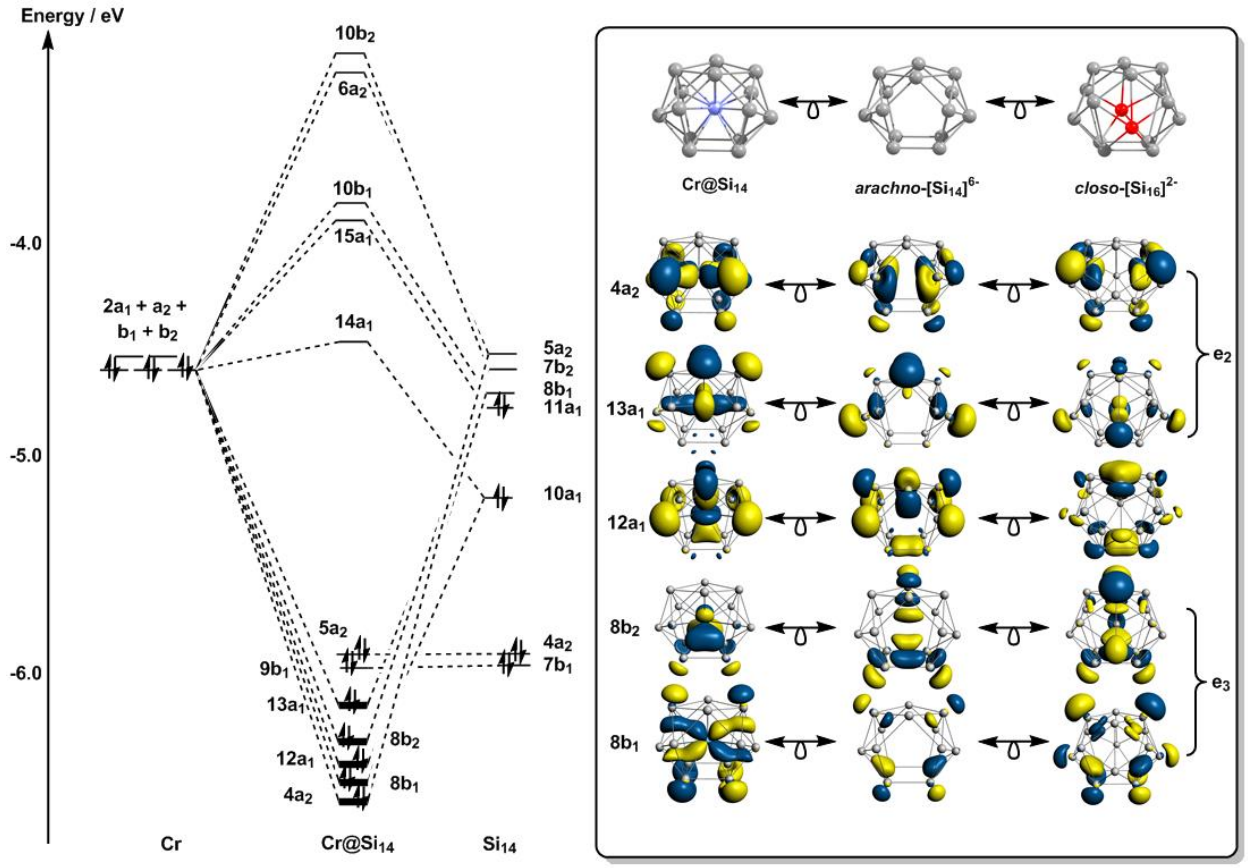

Figure 4 Kohn-Sham molecular orbitals for the "*arachno*" isomer, B, of $Cr@Si_{14}$ and the isolobal relationship between $Cr@Si_{14}$, *arachno*-$[Si_{14}]^{6-}$ and *closo*-$[Si_{16}]^{2-}$. e_2 and e_3 are degenerate representations of the D_{4d} point group.

precisely 62 valence electrons: indeed it makes little sense in qualitative terms for any other electron count. We can contrast this situation with isomer A, where three orbitals, 4e″ and 6a$_1$′, also accommodate six metal-based electrons. The difference is that the acceptor orbitals in isomer A are Si-Si π anti-bonding, and so the transfer of electron density from the metal destabilises the Si_{14} unit rather than stabilising it. The more integral role of the metal d electron density in isomer B compared to isomer A also lies behind the rapid destabilisation of the former as positive charge increases (Figure 2d-f). The dual role of the metal-based electrons in isomer B can be fulfilled only if the orbitals that are primarily metal-based maintain significant amplitude at the radius defined by the 14 silicon atoms – in other words, only if the isolobal analogies captured in the box in Figure 4 are valid. As the positive charge on the cluster increases, the metal d orbitals become increasingly contracted and the electrons in them less able to contribute to the stability of the Si_{14} unit. As a result, the stability of isomer B is much more strongly dependent on the charge than isomer A, where the d electrons play a less integral role in the cluster stability.

Octahedral Isomer C: The origin of the magic stability of the octahedral isomer C of $Fe@Si_{14}$ has been discussed at length in previous papers, most notably by Khanna and co-workers who considered in detail the relationship between geometry and stability.[22] Here we focus on the question of the role of the d electrons on the metal: are they integral to stability in the same way as they are isomer B? A significant clue comes from the work of King and co-workers[32] who identified the same octahedral isomer as the global minimum for the empty germanium cluster $[Ge_{14}]^{2-}$, suggesting a first-order description of $Fe@Si_{14}$ as $Fe^{2+}@\{Si_{14}\}^{2-}$. We can identify the 58 valence electrons of $[Si_{14}]^{2-}$ with the classic Wade's rules '*closo*' (= 4*n*+2) count, and indeed the high symmetry and high vertex connectivities (4 and 6) of isomer C are precisely the structural features that characterise highly electron-deficient *closo* boranes such as $[B_6H_6]^{2-}$. Based on this simple analysis, it

seems that the cage demands two, and only two, electrons from metal and not the full eight that are available in total from an Fe atom. The Kohn-Sham molecular orbital diagram in Figure 5 confirms this perspective: the $2e_g$ orbitals, which are an integral part of the 4n+2 = 58 *closo* electron count, carry substantial Fe-Si *and* Si-Si bonding character. They therefore play a similar dual role as the $8b_1$, $8b_2$ and $4a_2$ orbitals of isomer B, contributing simultaneously to electron count of the metal and to the characteristic electron count of the Si_{14} unit. The six remaining electrons of $Fe@Si_{14}$ are, however, surplus to the requirements, at least from the perspective of the Si_{14} cluster, and the $3t_{2g}$ orbital is Fe-Si antibonding: in effect, the *closo* $[Si_{14}]^{2-}$ unit acts as a π-donor ligand rather than as a π-acceptor. The anti-bonding character of the $3t_{2g}$ orbital is reflected in a comparison of the optimised structures of $Fe@Si_{14}$ and an empty $[Si_{14}]^{2-}$ cage (Figure 5): the Si atoms lying along the 3-fold rotation axes are forced away from the centre of the cluster in the presence of the metal (2.61 Å in $Fe@Si_{14}$ *vs* 2.44 Å in $[Si_{14}]^{2-}$).

The fact that the structure of isomer C is adapted to accommodate precisely two electrons from the metal accounts for its relative stability both at the start of the period and at the end, where low oxidation states dominate the chemistry. Early in the series this is simply because there are few electrons in the d orbitals, while at the end it is because the d orbitals have descended into the core and are therefore less available. We also note in this context that the plots for isomer A in Figure 2 d-f, in particular, are distinctly parabolic, indicating that its stability relative to C (recall that isomer C is chosen as the energetic reference) increases for both high negative and high positive charges. For the highly cationic species, the contraction of the d orbitals makes the electrons in the $2e_g$ orbital less able to fulfil their role in contributing to the $4n + 2$ count at the cluster, and so isomer C loses stability compared to isomer A (just as isomer B does, as discussed above). In the anionic regime, however, whilst the two electrons needed in the $2e_g$ orbital are certainly accessible, the radially expanded d orbitals magnify the antibonding character of the $3t_{2g}$ orbital, again destabilising isomer C relative to isomer A. Isomer C is therefore most stable in a relative sense around the middle of the series, where the metal d orbitals are diffuse enough to complete the $4n + 2$ count at the Si_{14} cage, but not so diffuse that the surplus electrons in the $3t_{2g}$ orbital become prohibitively destabilising.

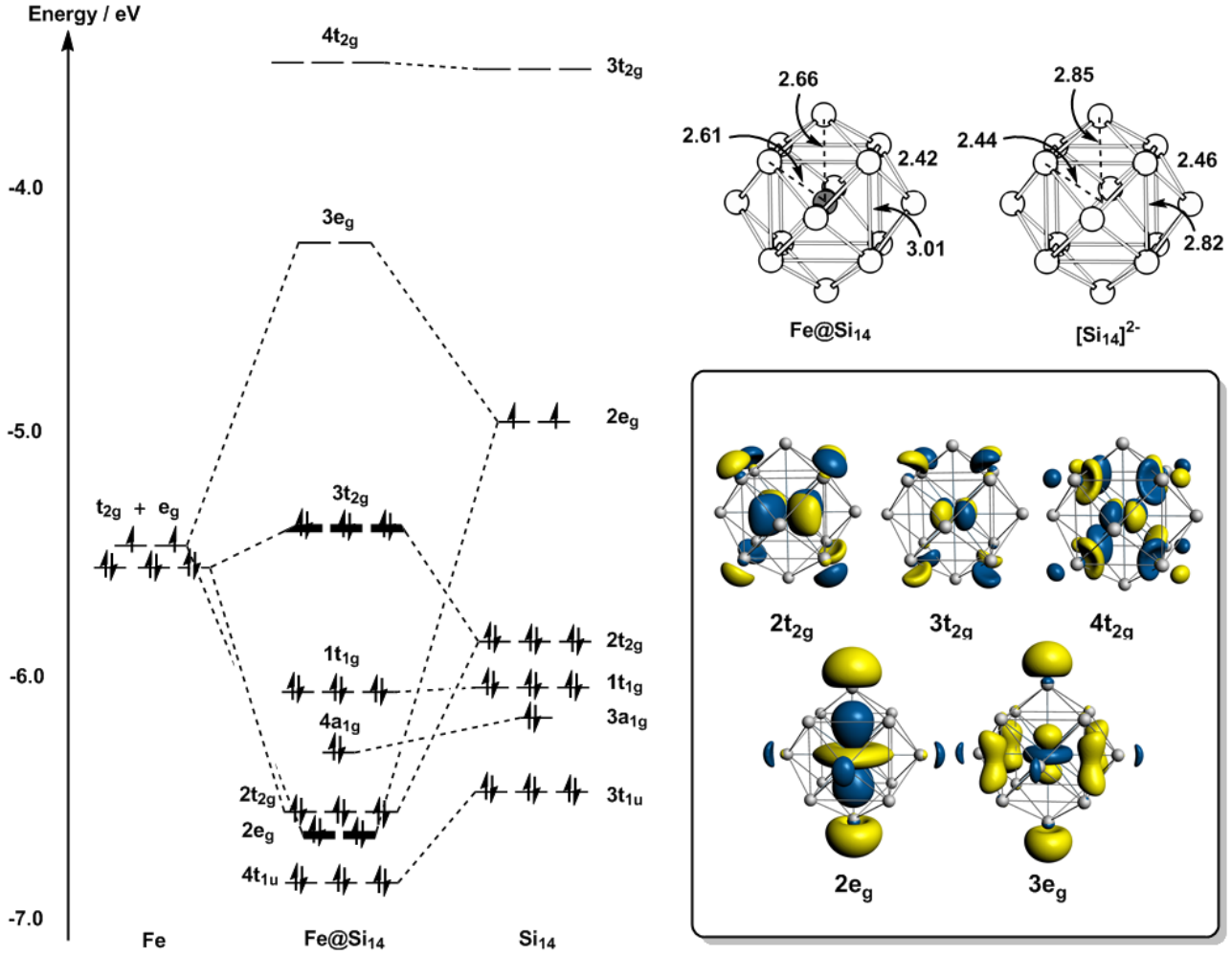

Figure 5 Kohn-Sham molecular orbitals for the "*closo*" octahedral isomer C of $Fe@Si_{14}$.

Journal Name

ARTICLE

Discussion and Summary

Our analysis of the electronic structure of the three isomers A, B and C shows that their relative stabilities reflect the ability of the metal to supply electron density to supplement the intrinsic 56-electron count of the empty Si_{14} cage. The structure of isomer C is characteristic of a 58-electron (*closo*-) count, and so it is specifically tailored to make use of two additional electrons from the metal: additional electrons in the $3t_{2g}$ orbital are surplus to requirements and weaken the interaction between the metal and the cage. The structure of isomer B, in contrast, is uniquely tailored to a 62-electron (*arachno*) count, and so needs six electrons from the metal. As a result of these different electronic demands, the stability of the isomer B is rapidly compromised relative to C by any factor that makes electrons on the metal less accessible: these factors can include (i) a reduction in the electron count (Figure 2a-c), (ii) an increase in positive charge (Figure 2d-f) or (iii) a change in functional. Isomer A is rather different from both B and C in so much as the characteristic 56-electron σ framework that is common to 'fullerene-like' and electron-precise clusters is not affected directly by the metal d electrons. This motif can accommodate up to six metal-based electrons through back-bonding to the Si-Si π* manifold, but the availability of electrons on the metal is not integral to stability in the same way as it is for either isomer B or C, and the structure is therefore more tolerant of a range of electron counts and charge states.

We noted from the outset that the "fullerene-like" and Wade's rules paradigms of cluster bonding are typically applied to very different families of clusters, and they rarely overlap. A link between the two models can, however, be established through a common electron-precise reference point (P_{14}, for example) with $5n$ = 70 valence electrons (second column of Figure 6).[33] These 70 electrons can be partitioned into $3n$ = 42 in the 21 σ bonds and $2n$ = 28 in the 14 radially directed lone pairs (or E-H bonding orbitals if the vertices are diatomic fragments such as B-H). This then leaves only two ways to accommodate lower electron counts: (i) depleting the electron density in the lone pairs with concomitant generation of multiple bonds (the "fullerene route", to left in Figure 6) or (ii) leaving the lone pairs intact and depleting the σ framework (the "Wade's rules route" to the right in Figure 6). The second option drives the characteristic formation of triangular faces and the increase in vertex connectivity that is the fingerprint of electron-deficiency. For any given electron count between the $4n$+2 and $5n$ limits, the "fullerene-like" and Wade's rules paradigms therefore represent alternative solutions to a common problem, of accommodating increasing electron deficiency. In carbon-based materials such as C_{60}, the strong 2p-2p π overlap and the low surface curvature combine to stabilise the π bonding orbitals, and so make the fullerene solution favourable. In the boranes, in contrast, depopulation of the radial orbitals is strongly disfavoured because these are in fact B-H bonding orbitals rather than lone pairs. Any reduction in electron count can therefore only be absorbed by depletion of the B-B σ framework (*i.e*. the Wade's rules route). The increasing stability of the ns^2np^2 configuration over ns^1np^3 down group 14 (the inert pair effect) has a similar effect, favouring double occupation of the radial orbital (the ns^2 lone pair), and hence the Wade's rules route over the fullerene alternative. As a result, the cluster chemistry of the heavier tetrels is dominated by deltahedral structures ($Ni@Pb_{12}$, $[Fe@Sn_{10}]^{3-}$, $[Mn@Pb_{12}]^{3-}$)[28,34,35] rather than fullerene-like alternatives. The endohedral silicon clusters appear to be rare intermediate cases where the two bonding paradigms collide, giving rise to near degenerate isomers which make use of the limited metal-based electron density available in fundamentally different ways. Whilst a thorough understanding of the factors that stabilise the different isomers brings us no closer to an answer to the question of which density functional is 'best', it does at least allow us to understand why functional roulette is such a dangerous game in the $M@Si_{14}$ family.

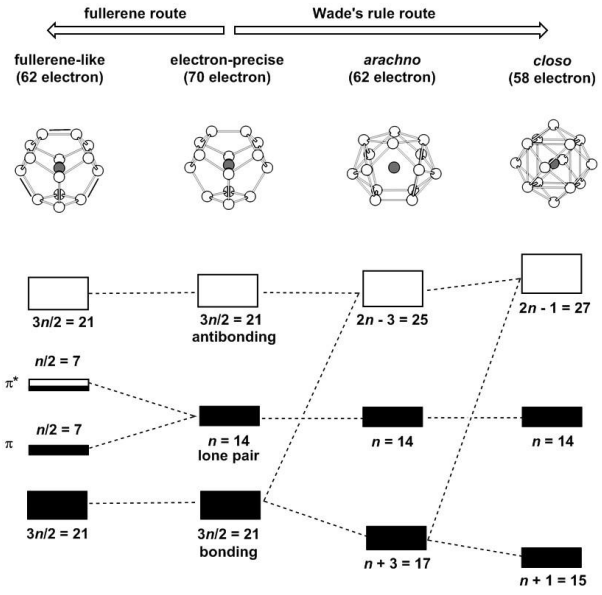

Figure 6: Schematic representation of the fullerene and Wade's rules routes to accommodating electron deficiency in $M@Si_{14}$ clusters. The numbers below each band indicate the number of orbitals.

Acknowledgements

We thank the EPSRC for financial support (JEM, VA, EP/K021435/1).

Computational methods

All DFT calculations described in this paper were performed with the Amsterdam Density Functional package (ADF2013.01)[36-38] using the gradient-corrected (GGA) functional proposed by Becke and Lee, Yang and Parr (BLYP)[39, 40] and the hybrid functional B3LYP.[41,42] An all electron Slater-type basis sets of triple-ζ quality, extended with a single polarisation function (TZP), was used to describe all metal atoms while DZP basis set was used to describe silicon atoms.[43] All structures were optimized using the gradient algorithm of Versluis and Ziegler.[44] The scalar relativistic zeroth-order regular approximation (ZORA) to the Dirac equation is used in all calculations.[45-49] The Conductor-like Screening Model (COSMO)[50-52] of solvation was applied for all calculations, and frequencies calculations were computed numerically.

Notes and references

1 S. M. Beck, *J. Chem. Phys.*, 1987, **87**, 4233-4234.
2 S. M. Beck, *J. Chem. Phys.*, 1989, **90**, 6306-6312.
3 M. Ohara, K. Koyasu, A. Nakajima and K. Kaya, *Chem. Phys. Lett.*, 2003, **371**, 490-497.
4 S. Neukermans, X. Wang, N. Veldeman, E. Janssens, R. E. Silverans and P. Lievens, *Int. J. Mass Spectrom.*, 2006, **252**, 145-150.
5 H. Hiura, T. Miyazaki and T. Kanayama, *Phys. Rev. Lett.*, 2001, **86**, 1733-1736.
6 P. Claes, E. Janssens, V. T. Ngan, P. Gruene, J. T. Lyon, D. J. Harding, A. Fielicke, M. T. Nguyen and P. Lievens, *Phys. Rev. Lett.*, 2011, **107**, 173401.
7 V. T. Ngan, E. Janssens, P. Claes, J. T. Lyon, A. Fielicke, M. T. Nguyen and P. Lievens, *Chem. Eur. J.*, 2012, **18**, 15788-15793.
8 W. Zheng, J. M. Nilles, D. Radisic and K. H. Bowen, Jr., *J. Chem. Phys.*, 2005, **122**, 071101.
9 J. M. Goicoechea and J. E. McGrady, *Dalton Trans.*, 2015, **44**, 6755-6766.
10 V. Arcisauskaite, X. Jin, J. M. Goicoechea and J. E. McGrady, in *Chemical Bond I: 100 Years Old and Getting Stronger*, ed. D. M. P. Mingos, Springer, New York, 2016, vol. 169, pp. 181-197.
11 V. Arcisauskaite, D. Fijan, M. Spivak, C. de Graaf and J. E. McGrady, *Phys. Chem. Chem. Phys.*, 2016, **18**, 24006-24014.
12 S. N. Khanna, B. K. Rao and P. Jena, *Phys. Rev. Lett.*, 2002, **89**, 016803.
13 R. B. King, in *Zintl Ions: Principles and Recent Developments*, ed. T. F. Fassler, Springer-Verlag Berlin, Berlin, 2011, vol. 140, pp. 1-24.
14 R. B. King, I. Silaghi-Dumitrescu and M. M. Uta, *Dalton Trans*, 2007, 364-372.
15 J. Ulises Reveles and S. N. Khanna, *Phys. Rev. B*, 2005, **72**, 165413.
16 J. Ulises Reveles and S. N. Khanna, *Phys. Rev. B*, 2006, **74**, 035435.
17 M. B. Abreu, A. C. Reber and S. N. Khanna, *J. Phys. Chem. Lett.*, 2014, **5**, 3492-3496.
18 T. Miyazaki, H. Hiura and T. Kanayama, *Phys. Rev. B*, 2002, **66**, 121403.
19 V. Kumar and Y. Kawazoe, *Phys. Rev. B*, 2002, **65**, 073404.
20 J. Lu and S. Nagase, *Phys. Rev. Lett.*, 2003, **90**, 115506.
21 J. He, K. Wu, C. Liu and R. Sa, *Chem. Phys. Lett.*, 2009, **483**, 30-34.
22 V. Chauhan, M. B. Abreu, A. C. Reber and S. N. Khanna, *Phys. Chem. Chem. Phys.*, 2015, **17**, 15718-15724.
23 V. Kumar and Y. Kawazoe, *Phys. Rev. Lett.*, 2001, **87**, 045503.
24 V. T. Ngan, K. Pierloot and M. T. Nguyen, *Phys. Chem. Chem. Phys.*, 2013, **15**, 5493-5498.
25 H. T. Pham, H. T. Nguyen and M. T. Nguyen, *Struct. Chem.*, 2017, DOI: 10.1007/s11224-017-0973-4.
26 M. G. Medvedev, I. S. Bushmarinov, J. W. Sun, J. P. Perdew and K. A. Lyssenko, *Science*, 2017, **355**, 49-52.
27 S. Hammes-Schiffer, *Science*, 2017, **355**, 28-29.
28 T. Krämer, J. C. Duckworth, M. D. Ingram, B. Zhou, J. E. McGrady and J. M. Goicoechea, *Dalton Trans*, 2013, **42**, 12120-12129.
29 R. O. Jones and G. Seifert, *Phys. Rev. Lett.*, 1997, **79**, 443-446.
30 M. Häser, U. Schneifer and R. Ahlrichs, *J. Am. Chem. Soc.*, 1992, **114**, 9551-9559.
31 P. von Ragué Schleyer, K. Najafian and A. M. Mebel, *Inorg. Chem.*, 1998, **37**, 6765-6772.
32 R. B. King, I. Silaghi-Dumitrescu and M. M. Uţă, *Eur. J. Inorg. Chem.*, 2008, **2008**, 3996-4003.
33 J. E. McGrady, *J. Chem. Ed.*, 2004, **81**, 733-737.
34 E. N. Esenturk, J. Fettinger and B. Eichhorn, *J. Am. Chem. Soc.*, 2006, **128**, 9178-9186.
35 B. Zhou, T. Krämer, A. L. Thompson, J. E. McGrady and J. M. Goicoechea, *Inorg. Chem.*, 2011, **50**, 8028-8037.
36 G. Te Velde, F. M. Bickelhaupt, E. J. Baerends, C. Fonseca Guerra, S. J. A. Van Gisbergen, J. G. Snijders and T. Ziegler, *J. Comput. Chem.*, 2001, **22**, 931-967.
37 C. Fonseca Guerra, J. G. Snijders, G. Te Velde and E. J. Baerends, *Theor. Chem. Acc.*, 1998, **99**, 391-403.
38 E. J. Baerends, SCM, Theoretical chemistry, Vrije Universiteit, Amsterdam, The Netherlands, ADF2013, http://www.scm.com.
39 A. D. Becke, *Phys. Rev. A*, 1988, **38**, 3098-3100.
40 C. Lee, W. Yang and R. G. Parr, *Phys. Rev. B*, 1988, **37**, 785-789.
41 A. D. Becke, *J. Chem. Phys.*, 1993, **98**, 5648-5652.
42 P. J. Stephens, F. J. Devlin, C. F. Chabalowski and M. J. Frisch, *J. Phys. Chem.*, 1994, **98**, 11623-11627.
43 E. Van Lenthe and E. J. Baerends, *J. Comput. Chem.*, 2003, **24**, 1142-1156.
44 L. Versluis and T. Ziegler, *J. Chem. Phys.*, 1988, **88**, 322.
45 E. van Lenthe, E. J. Baerends and J. G. Snijders, *J. Chem. Phys.*, 1993, **99**, 4597-4610.
46 E. van Lenthe, E. J. Baerends and J. G. Snijders, *J. Chem. Phys.*, 1994, **101**, 9783-9792.
47 E. van Lenthe, J. G. Snijders and E. J. Baerends, *J. Chem. Phys.*, 1996, **105**, 6505-6516.
48 E. van Lenthe, R. van Leeuwen, E. J. Baerends and J. G. Snijders, *Int. J. Quantum Chem.*, 1996, **57**, 281-293.
49 E. van Lenthe, A. Ehlers and E.-J. Baerends, *J. Chem. Phys.*, 1999, **110**, 8943-8953.
50 A. Klamt and G. Schüürmann, *J. Chem. Soc., Perkin Trans. 2*, 1993, 799-805.
51 A. Klamt, *J. Phys. Chem.*, 1995, **99**, 2224-2235.
52 A. Klamt and V. Jonas, *J. Chem. Phys.*, 1996, **105**, 9972-9981.